Chemical Engineering Journal xxx (xxxx) xxx–xxx

Contents lists available at ScienceDirect

Chemical Engineering Journal

journal homepage: www.elsevier.com/locate/cej

# Preparation of carbon supported Pt-Ni alloy nanoparticle catalyst with high metal loading using cation exchange resin and its application for hydrogen production

Supanat Hanprerakriengkrai[a], Hiroyasu Fujitsuka[a,*], Koji Nakagawa[a], Hiroyuki Nakagawa[b], Teruoki Tago[a]

[a] Department of Chemical Science and Technology, Tokyo Institute of Technology, 2-12-1, Ookayama, Meguro-ku, Tokyo 152-8552, Japan
[b] Department of Chemical Engineering, Kyoto University, Kyotodaigaku-katsura, Nishikyo-ku 615-8510, Japan

## HIGHLIGHTS

- Carbon supported Pt-Ni catalysts were prepared from a cation-exchange resin.
- The Pt-Ni/Cs possessed high metal loading and small metal alloy particles.
- Pt-Ni/Cs exhibited higher catalytic activity in formic acid decomposition than Pt/C.
- Metal surface area was improved by a supercritical water treatment at 400 °C for 1 h.

## GRAPHICAL ABSTRACT

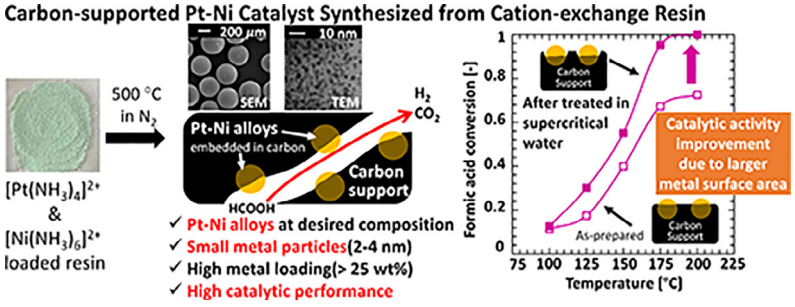


## ARTICLE INFO

*Keywords:*
Ion-exchange resin
Carbon supported Pt-Ni alloy catalyst
Formic acid decomposition
Hydrogen production

## ABSTRACT

Formic acid has been attracting interest as a promising hydrogen carrier because hydrogen can be produced over the catalysts under mild condition with low energy input. Though the catalytic activity for hydrogen production from formic acid is enhanced by increasing the metal loading, the trade-off between high metal loading and small metal particle size practically occurred with carbon catalyst prepared by impregnation method. To overcome this challenge, we herein utilized a noble catalyst preparation method which uses an ion-exchange resin as an initial carbon material. Five compositions of carbon supported Pt-Ni alloy catalysts were successfully prepared at high metal loading (25–50 wt%) with small metal particle sizes (2.3–3.8 nm observed by TEM). The metal particles were embedded in the carbon, which was contributed to small particle size of the loaded metal. The hydrogen production from formic acid was investigated over the prepared catalysts at 100–200 °C. It was elucidated that the turnover frequencies of $Pt_{50}Ni_{50}$/C and $Pt_{75}Ni_{25}$/C were higher than that of Pt/C at above 175 °C, suggesting that the decrease of Pt content without losing their catalytic activity could be achieved by $Pt_{50}Ni_{50}$/C and $Pt_{75}Ni_{25}$/C due to alloy formation. To further enhance the catalytic activity by increasing the active metal surface area, supercritical water treatment at 400 °C for 1 h was utilized. The metal surface area of catalysts was noticeably increased due to the gasification of the carbon support nearby metal particles. Formic acid conversion, likewise, drastically increased after the treatment.

* Corresponding author.
*E-mail address:* fujitsuka@cap.mac.titech.ac.jp (H. Fujitsuka).

https://doi.org/10.1016/j.cej.2018.10.213

## 1. Introduction

Hydrogen has attracted an extensive consideration as an economical, sustainable and clean energy carrier. It furthermore has been numerously utilized as a feedstock in various chemical processes particularly in crude oil handling and petrochemical production [1–3]. Despite the widespread applications of hydrogen, the transportation and storage of hydrogen are difficult. To overcome this problem, the utilization of hydrogen carriers has been emphasized a promising strategies [4–10]. Formic acid has recently received extensive attention and has become a potential hydrogen carrier because formic acid is easy to handle, has high hydrogen capacity, and can be formed via catalytic conversion under mild condition [6–8].

Hydrogen production via formic acid decomposition, presently, has been extensively researched over various species of active metals, both of noble and non-noble metals, including Pt [5,10–16], Ni [17–20] and their alloys [21]. Low catalytic activity, nevertheless, is consistently obtained from hydrogen production via formic acid decomposition under low temperature [7–9]. For the enhancement of the catalytic activity, the two approaches have been performed. One approach is to enhance the catalytic activity by modifying the active site chemical structure such as utilizing alloy metals. Electronic structure can be modified by alloy formation, leading to the catalytic enhancement. Many researches have been reported that the Pt-Ni alloy catalysts exhibited the higher catalytic activity for various reactions, such as formic acid electrooxidation [21] and dehydrogenation of hydrocarbons [22,23], than single Pt catalysts. It was visualized that the utilization of Pt-Ni alloy might presumably enhance the catalytic activity of hydrogen production via formic acid decomposition over a carbon supported metal catalyst.

The other approaches for the enhancement of catalytic activity is the increasing the active metal surface by increasing metal loading and decreasing the active metal particle size. Though the catalytic activity based on the catalyst weight is enhanced by increasing metal loading and reducing metal particle size, the common trade-off between these approaches is practically experienced. A metal particle size generally increases with a metal loading, particularly preparing via impregnation method at high metal loading, resulting in reducing a concentration of surface metal site and in lower turnover frequencies for hydrogen production [7–9]. Hence, the preparation of fine metal particle catalysts using stabilizing agents has been studied [24–26]. Dispersing and stabilizing metallic particle can be practicably performed over the various modified carbon materials, e.g. carbon nanotube [27,28] and N-doped carbon [10–14]. Nevertheless, due to the complicated preparation procedures, which requires both in support pretreatment and metal loading step, and synthetic chemicals, it is difficult to apply these preparation methods for the industrial use. Thus the development of the simple preparation method for metal loaded carbon catalysts at high metal loading with small metal particle size is required.

To overcome the common trade-off between high metal loading and small metal particle size, the authors have proposed the novel and straightforward preparation method for carbon-supported monometallic catalyst, namely carbon-supported Pt [29] and Ni [30–32] catalysts. This preparation method consists of two steps; ion-exchange step to load metal ion on the ion-exchange resin and carbonization step to convert the resin into carbon and reduce the metal from ionic to metallic state. The 50 wt% Ni loaded carbon catalyst with metal particle size of 3 nm was synthesized by this method and showed high activity in hydrogen production via hydrothermal gasification as reported by Nakagawa et al. [30–32]. In this article, we extend this preparation method to synthesize high metal loading carbon supported Pt-Ni alloy catalysts with fine particles by treating the ion-exchange resin with the same type of metal ions, namely $[Pt(NH_3)_4]^{2+}$ and $[Ni(NH_3)_6]^{2+}$, which are stable in the ion-exchange solution. This demonstrates the potential for preparing the carbon supported Pt-Ni alloy catalysts by using cation-exchange resin, which has not been presented elsewhere.

Herein, several compositions of carbon supported Pt-Ni alloy catalysts, Pt/C, $Pt_{75}Ni_{25}$, $Pt_{50}Ni_{50}$, $Pt_{25}Ni_{75}$ and Ni/C, were prepared at high metal loading, using cation-exchange resin as a carbon precursor, and utilized in hydrogen production via formic acid decomposition. To further enhance the catalytic activity for the formic acid decomposition, supercritical water treatment was applied with the prepared catalysts for physical properties improvement and compared with the untreated one.

## 2. Experimental

### 2.1. Catalyst preparation

The catalyst preparation method using an ion-exchange resin reported by Nakagawa et al. [32–34] was modified to prepare the carbon-supported catalysts containing Pt and Ni. Five types of carbon-supported metal catalysts, Pt/C, $Pt_{75}Ni_{25}$/C, $Pt_{50}Ni_{50}$/C, $Pt_{25}Ni_{75}$/C, and Ni/C, were prepared by using a weakly acidic cation-exchange resin, WK-11 (Mitsubishi Chemical, Japan), $Pt(NH_3)_4Cl_2{\cdot}H_2O$ (98% in purity, Wako Pure Chemical Ltd., Japan), and $Ni(NO_3)_2{\cdot}6H_2O$ (98% in purity, Wako Pure Chemical Ltd., Japan) as a carbon material, Pt precursor, and Ni precursor. 3 g of the cation-exchange resin was put into 100 mL of distilled water. The pH value of the solution was then adjusted at 8.8 by 28 wt% ammonia aqueous solution (Wako Pure Chemical Ltd., Japan) with stirring. The same volume of bimetallic aqueous solution with a predetermined concentration was prepared. The molar composition of metal was fixed at Pt:Ni = 100:0, 75:25, 50:50, 25:75, and 0:100. The metal solution was added dropwise into the cation-exchange resin solution to perform an ion-exchange process. The molar ratio of metal to ion-exchange site and the initial metal concentration in the ion-exchange solution was respectively fixed at 0.25 and 7.5 mM for all samples. It was continuously stirred at room temperature for 24 h. The pH value was repeatedly adjusted at 8.8 by $NH_3$ aqueous solution at 2 and 4 h after adding the metal solution. The metal loaded resin was collected and dried overnight at room temperature. The metal loaded carbon catalysts were finally obtained by carbonization at 500 °C for 30 min in $N_2$ atmosphere, where the resin was pyrolyzed to form carbon and the metal ions were reduced to form metal nanoparticles.

Aiming to further enhance the catalytic performance, a supercritical water treatment (ScWT) was carried to increase the active metal surface area of the prepared catalysts. Typically, 1 g of the prepared catalyst was put into a 7 mL of stainless batch vessel filled with distilled water. The sample in the closed vessel was then treated in an electric furnace for 1 h at 400 °C, where the vessel inside was pressurized by an autogenous pressure. After the treatment, the vessel was quenched in ice bath, and the treated catalyst was collected and dried at 110 °C for 30 min. The catalysts with ScWT were labeled by adding “ScWT” to the original catalyst such as “$Pt_{50}Ni_{50}$/C-ScWT”.

### 2.2. Catalyst characterization

The metal loading of carbon-supported catalysts were estimated from weight of the remaining ashes after combustion with Thermo plus Evo2 TG8120 (Rigaku, Japan) at 900 °C in an air stream for 20 min by assuming that the remained ashes consist of Pt and NiO. Metal composition was determined by an inductively coupled plasma optical emission spectrometry (ICP-OES; 5100 VDV, Agilent Technologies Japan, Ltd.) The morphology of the catalysts was observed by a scanning electron microscopy (SEM; VE-9800, Keyence Corp., Japan) at 8 kV. $N_2$ adsorption was conducted at 77 K with Belsorp-mini High Precision Volumetric Gas Adsorption Analyzer (MicrotracBEL Japan, Inc.) to analyze Brunauer-Emmett-Teller (BET) surface area, $S_{BET}$, and micro pore volume of catalysts.

CO pulsed chemisorption at 50 °C was performed with BEL-METAL (MicrotracBEL Japan, Inc.) to evaluate metal surface area. The molar ratio of absorbed CO to an active metal Pt and Ni was assumed to be

1:1. The metal particle size was estimated by three different methods; the CO pulsed chemisorption, a transmission electron microscopy (TEM; H-7650 Zero.A, Hitachi High-Technology, Japan) at 120 kV, and a powder X-ray diffraction spectrometry (XRD; Miniflex 600, Rigaku, Japan) with Cu-Kα radiation (λ = 1.5418 Å) operated at 40 kV and 15 mA, 0.02° step, and 10°/min scan speed. XRD measurement was also used for crystal structure analysis.

Metal accessibility is defined by the ratio of the accessible metal surface area evaluated by CO pulsed chemisorption ($S_{metal,\ CO}$) to the geometrical surface area calculated by metal particle size observed by TEM ($S_{metal,\ TEM}$). $S_{metal,\ CO}$ is calculated as

$$\text{Smetal, CO} = \frac{w}{\rho}\frac{6}{\pi {d_{CO}}^3}\pi {d_{CO}}^2 \quad (1)$$

where $w$ is metal loading [g-metal/g-cat], ρis density of metal [g/nm$^3$], and $d_{CO}$ is metal particle size obtained by CO pulsed chemisorption [nm]. In the same manner, $S_{metal,\ TEM}$ is calculated as

$$\text{Smetal, TEM} = \frac{w}{\rho}\frac{6}{\pi {d_{TEM}}^3}\pi {d_{TEM}}^2 \quad (2)$$

where $d_{TEM}$ is metal particle size obtained by TEM observation [nm]. The metal accessibility is therefore formulated as Eq. (3).

$$\text{Metalaccessibility}[\%] = \frac{\text{Smetal, CO}}{\text{Smetal, TEM}} \times 100 = \frac{d_{TEM}}{d_{CO}} \times 100 \quad (3)$$

### 2.3. Catalytic activity test

Hydrogen production via formic acid decomposition was performed to assess catalytic activities of all samples. The catalyst homogeneously mixed with glass beads to avoid reactant by-passing was loaded in a quartz tube flow reactor (4.5 mm i.d.) to achieve 5 mm height. The catalyst in the reactor was pretreated in 10% $H_2/N_2$ stream at 350 °C and was cooled to 100 °C. Formic acid was fed into the preheater at 1 mL-liq/h by a syringe pump and supplied to the reactor in gas phase with 79.2 mL/min of $N_2$. The *W/F* (i. e., contact time) was controlled at 0.004 h·$g_{Metal}/g_{HCOOH}$. The reaction temperature was increased by 25 °C from 100 to 200 °C at the interval of 80 min after formic acid was fed. The product gas was quantitatively analyzed at every 30 min after the temperature was changed (i. e., 30, 110, 190, 270, and 350 min of time on streams (TOSs) for 100, 125, 150, 175, and 200 °C of reaction temperature, respectively) by an on-line gas chromatography (GC-2014, SHIMADZU Corp., Japan) equipped with a Shincarbon ST column (Shinwa Chemical Industries Ltd., Japan) and a thermal conductivity detector. As discussed later in Sections 3. 2 and 3.3, no catalytic deactivation was observed throughout the reaction experiments. The formic acid conversion was calculated by the molar ratio of CO and $CO_2$ generated to formic acid fed to the reactor. The hydrogen selectivity was determined by the ratio of the molar quantity of hydrogen produced to the sum of that of CO and $CO_2$. The turnover frequency (TOF) at 30 min after the temperature change was estimated by using a number of active metal atoms assessed by the CO pulsed chemisorption.

For durability test, 510 min of the reaction was performed over $Pt_{75}Ni_{25}$/C at 175 °C with the same feed composition and contact time as the catalytic activity test.

## 3. Results and discussion

### 3.1. Properties of prepared catalysts

The characteristics of the catalysts prepared are listed in Table 1. The spherical carbon supported catalysts with the diameter of 200–500 μm were obtained as displayed in Fig. 1. The spherical shape was maintained after the carbonization. As evident from Table 1, the metal loadings of all prepared carbon supported catalysts were higher than 25 wt%. As the molar proportion of metal to ion-exchange site and metal ion concentration were fixed, the metal loading monotonically increased with increasing Pt composition, up to 50 wt%, due to the larger molecular weight of Pt than Ni. The metal composition of Pt and Ni in Pt-Ni/Cs measured by the ICP-OES was same to the initial composition in the ion-exchange solution, indicating that the metal ion was completely adsorbed onto the ion-exchange resin. The $S_{BET}$ and micropore volume were observed in range of 270–310 $m^2/g_{cat}$ and 0.12–0.13 $cm^3/g_{cat}$, respectively, which were drastically larger than those of initial ion-exchange resin (5.7 $m^2/g$ and 0.002 $cm^3/g$). The pore development during carbonization might be attributed to the removal of low molecular weight gaseous e.g. $H_2$, $CO_2$, CO, and some hydrocarbons produced in the process. From these results, the carbon-supported bimetallic catalysts at high metal loading was achieved by treating the ion-exchange resin with the bimetal ion containing solution, followed by the carbonization.

Because it was elucidated that both Pt and Ni were loaded on the Pt-Ni/Cs, the state of loaded metals was investigated by XRD analysis and TEM observation. The XRD patterns of the prepared catalysts were shown in Fig. 2. The broad peaks observed in this figure indicate that the small metal particles were highly dispersed in all prepared catalysts. For the carbon supported monometallic catalysts, Pt/C and Ni/C, the observed peaks were consistent with those of the corresponding metals, indicating that both Pt and Ni were loaded as metallic Pt and Ni, respectively. The observed peaks of the carbon-supported bimetallic catalysts, on the other hand, were consistent with neither Pt nor Ni characteristic peaks and shifted monotonically to higher angle with increasing Ni composition. This peak shift indicates that Pt-Ni alloy metal was formed during the preparation of Pt-Ni/Cs. During the carbonization step, metal ions in the resin would be reduced to metallic state and aggregated to form metal nanoparticles. Thus, for the Pt-Ni/Cs, Pt and Ni were aggregated at random, resulting in the alloy formation during the carbonization step. This higher angle shifts of the Pt peaks was also observed after the alloy formation with Ni in the literature [21,23,33,34], in which the alloy structure was confirmed by a scanning transmission electron microscopy complemented with electron energy loss spectroscopy (STEM-EELS) [33] and an X-ray photoelectron spectroscopy (XPS) [34]. In addition, the lattice constants of $Pt_{75}Ni_{25}$/C, $Pt_{50}Ni_{50}$/C, and $Pt_{25}Ni_{75}$/C were estimated at 0.226, 0.223, and 0.217 nm, which were consistent with those obtained from Vegard's law. Because the peak position of our Pt-Ni bimetallic catalysts was the same as both those of the literature and the estimated value, we concluded the Pt-Ni metals in our catalysts possessed the alloy structure. By using Scherrer equation ($d_{XRD} = K\lambda/B\cos\theta$ where $K$ is 0.9), the average sizes of Pt-Ni alloy particles were estimated at 1.6–2.3 nm as listed in Table 1. These results were confirmed by the TEM observation (Fig. 3a) showing comparable metal particle sizes around 3 nm. The evidence presented here apparently demonstrates that the carbon supported Pt-Ni alloy catalysts at high metal loading with fine metal particles were successfully synthesized by using cation-exchange resin as a precursor.

To study thoroughly the metal structure of prepared catalysts, the comparison of $d_{CO}$ and $d_{XRD}$ was concerned. As can be seen in Table 1, $d_{CO}$ which was estimated from the accessible metal surface area was relatively larger (8.3–83.7 nm) than $d_{TEM}$ which represents the geometric metal particle size. This difference suggests that the metal particles of the prepared catalysts were partially embedded in a carbon support. Although the metal accessibility, was estimated at 4.5–35.0%, the immobilization state of metal particles contributed to small sizes of approximately 3 nm.

### 3.2. The catalytic activity test on hydrogen production via formic acid decomposition

Fig. 4 (a) illustrate the conversion in formic acid decomposition over the prepared Pt-Ni/Cs as a function of reaction temperature (100–200 °C). Hydrogen production proceeded above 100 °C over Pt/C

**Table 1**
Metal and pore structure properties of the prepared carbon supported metal catalysts without and with ScWT at 400 °C for 1 h.

| | Metal loading [wt%] | Pt composition[mol %] | Metal surface area [$m^2/g_{cat}$] | Metal particle size [nm] | | | Metal accessibility[a] [%] | BET surface area [$m^2/g_{cat}$] | Micropore volume[b] [$cm^3/g_{cat}$] |
|---|---|---|---|---|---|---|---|---|---|
| | | | | $d_{CO}$ | $d_{XRD}$ | $d_{TEM}$ | | | |
| Pt/C | 49.4 | 100 | 16.7 | 8.3 | 2.2 | 2.9 | 35.0 | 274 | 0.13 |
| Pt/C-ScWT | 49.2 | 100 | 20.3 | 6.8 | 2.4 | 2.9 | 42.7 | 301 | 0.13 |
| $Pt_{75}Ni_{25}$/C | 42.8 | 74.6 | 9.6 | 13.2 | 1.8 | 2.6 | 19.7 | 307 | 0.13 |
| $Pt_{75}Ni_{25}$/C-ScWT | 40.0 | 76.3 | 13.9 | 8.5 | 1.8 | 2.8 | 32.9 | 344 | 0.14 |
| $Pt_{50}Ni_{50}$/C | 36.4 | 50.0 | 6.1 | 19.3 | 1.6 | 2.4 | 12.5 | 293 | 0.12 |
| $Pt_{50}Ni_{50}$/C-ScWT | 38.4 | 52.3 | 11.0 | 11.3 | 1.7 | 2.7 | 23.9 | 328 | 0.14 |
| $Pt_{25}Ni_{75}$/C | 31.9 | 25.0 | 2.9 | 42.4 | 2.3 | 2.3 | 5.4 | 279 | 0.12 |
| $Pt_{25}Ni_{75}$/C-ScWT | 32.2 | 28.5 | 6.3 | 19.8 | 2.4 | 2.7 | 13.6 | 304 | 0.13 |
| Ni/C | 25.4 | 0 | 2.0 | 83.7 | 1.7 | 3.8 | 4.5 | 253 | 0.12 |
| Ni/C-ScWT | 27.7 | 0 | 4.0 | 46.5 | 1.7 | 3.9 | 8.4 | 304 | 0.13 |

[a] Estimated by using Eq. (3)
[b] Estimated based on the t-plot method.

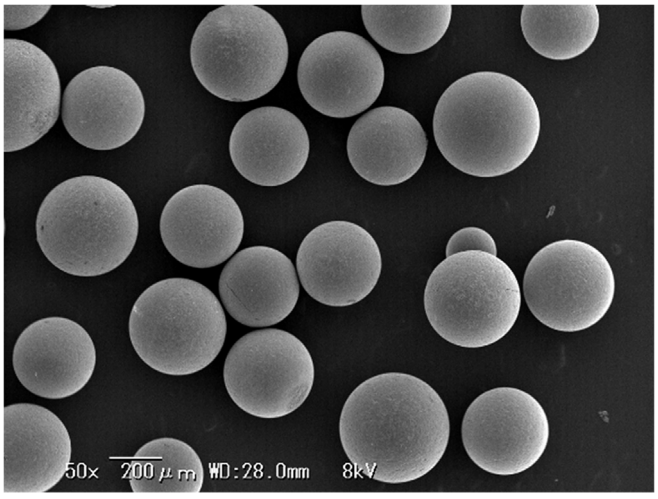


**Fig. 1.** SEM image of prepared $Pt_{50}Ni_{50}$/C (×200).

and Pt-Ni/Cs, while it proceeded above 125 °C over Ni/C. Concerning the catalytic performance of the prepared Pt-Ni alloy catalysts, it is not surprising that the conversion in formic acid decomposition obviously increased with increasing Pt composition and reaction temperature. As compared the catalytic activity in formic acid conversion of the prepared catalysts with the literature [5,14], our prepared catalysts yielded a slightly higher conversion of formic acid decomposition in gaseous phase even though the smaller contact time (0.004 $h{\cdot}g_{metal}/g_{HCOOH}$) was used. For instance, the formic acid conversion observed over the prepared Pt/C catalyst at 150 °C was 0.73, whereas those observed over the Pt/C catalysts were reported at 0.38 (0.006 $h{\cdot}g_{metal}/g_{HCOOH}$) [14] and 0.52 (0.1 $h{\cdot}g_{metal}/g_{HCOOH}$) [5].

For all the experiment, $H_2$, $CO_2$ and a little quantity of CO were detected and therefore the dehydrogenation of formic acid (Eq. (4)) and the dehydration of formic acid (Eq. (5)) were observed during the reaction.

$$HCOOH \leftrightarrow H_2 + CO_2 \quad (4)$$

$$HCOOH \leftrightarrow H_2\ O + CO \quad (5)$$

$$H_2 + CO_2 \leftrightarrow H_2\ O + CO \quad (6)$$

The hydrogen selectivity was over 80% for all of the experiments and moderately increased with increasing Pt composition as shown in Fig. 4(b). It, nevertheless, was not substantially influenced by the reaction temperature. It is commonly accepted that the reverse water-gas

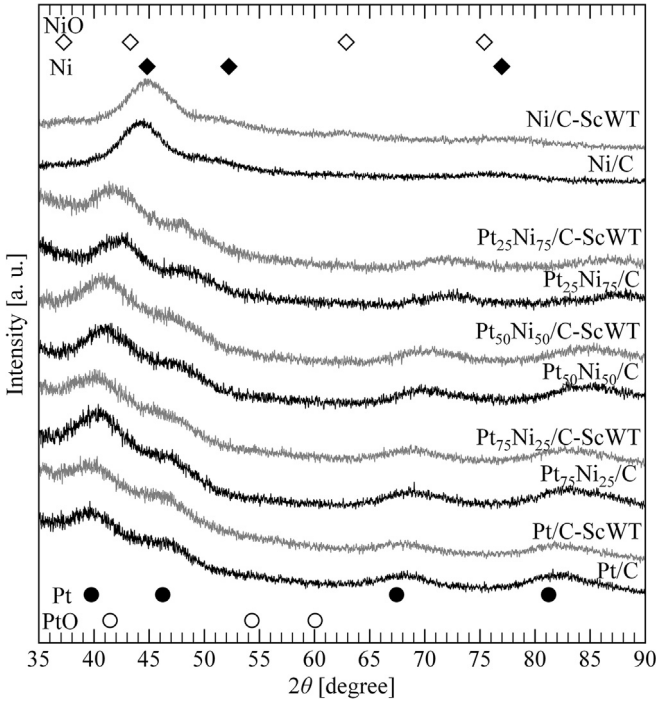


**Fig. 2.** XRD patterns of the prepared carbon supported metal catalysts without and with ScWT at 400 °C for 1 h with characteristic peaks of Pt (●), PtO(○), Ni (♦) and NiO(◊).

shift reaction (RWGSR; Eq (6)) concurrently proceeds with formic acid decomposition. To validate that the observed hydrogen selectivity was not dominantly influenced by the contribution of RWGSR, an equilibrium hydrogen selectivity ($S_{H2,\ RWGSR}$) was calculated, which was plotted as the dashed line in Fig. 4(b). The hydrogen selectivities observed were not consistent with the equilibrium value for all prepared catalysts. Furthermore, the lower hydrogen selectivity, compared with equilibrium selectivity, was observed over Pt/C and $Pt_{75}Ni_{25}$/C at temperatures below 125 °C, while it overreached the equilibrium selectivity at temperatures above 150 °C. This result apparently indicates that the hydrogen selectivity was not thermodynamically determined by RWGSR. The difference in hydrogen selectivity could then be attributed to the adsorption state of formic acid. It was reported that hydrogen and carbon dioxide were dominantly produced via the bridging formate species [35], whereas carbon monoxide and water were produced via the linear one [36]. As reported by Luo et al. [37], the

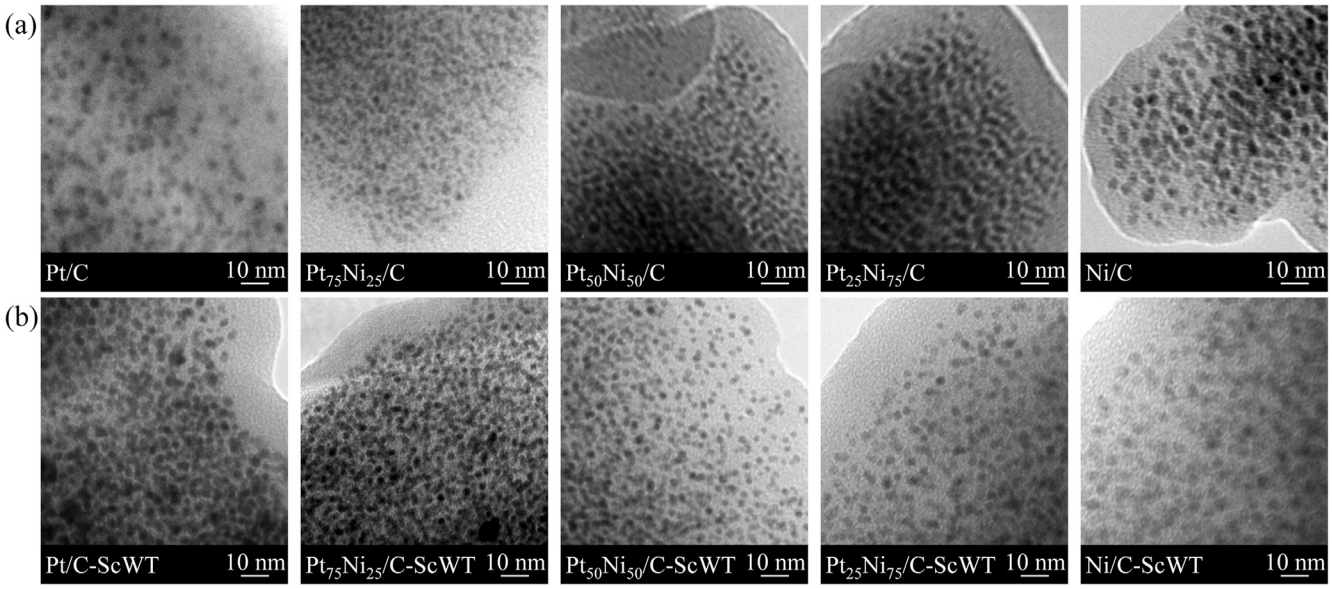


**Fig. 3.** TEM image of (a) untreated and (b) treated carbon supported Pt-Ni alloy catalysts with ScWT at 400 °C for 1 h.

three adsorption state of formic acid on Ni, the formate, the linear structure with one oxygen atom at atop site, and the linear structure with threefold capping, were observed, while only the bridging formate structure was found on Pt. Therefore, the higher hydrogen selectivity could be observed over Pt/C rather than Ni/C, which was agreement with our observations. The hydrogen selectivity of Pt-Ni/Cs, likewise, increased with Pt composition.

Next, the stability of the Pt-Ni alloy catalysts was examined by the characterization of the spent catalysts and the long term catalytic reaction. The XRD spectra of the Pt-Ni/Cs before and after the catalytic reaction was displayed in Fig. 5. The broad peaks observed over spent Pt-Ni/Cs in this figure indicate that the metal particles still remained small and highly dispersed. There was no peak shift observed over the spent Pt-Ni/Cs, suggesting that alloy structure was maintained through the catalytic reaction. Likewise, the metal loading of spent Pt-Ni/Cs was not drastically changed as listed in Table 2. These results evidently confirm that the Pt-Ni alloy crystal structure was not changed after the reaction. Furthermore, the metal particle sizes of the fresh and the spent Pt-Ni/Cs were similar, suggesting that there was no metal aggregation during reaction. This high stability of the fine Pt-Ni alloy metals can be because of the contribution of metal particle embedded structure. The long term catalytic reaction was performed over $Pt_{75}Ni_{25}$/C at 175 °C for 510 min. Both the formic acid conversion and the hydrogen selectivity were almost constant against the time on stream over 510 min as shown in Fig. 6 and no significant catalytic deactivation was observed.

To study thoroughly the catalytic activity on hydrogen production via formic acid decomposition, varied in different ratios of active metals, the turnover frequency (TOF) was estimated by using the number of accessible active sites observed with CO pulsed chemisorption. The Arrhenius plot of turnover frequencies of prepared catalysts was depicted in Fig. 4(c). Despite the highest formic acid conversion was observed over Pt/C, the TOFs of $Pt_{50}Ni_{50}$/C and $Pt_{75}Ni_{25}$/C (2.48 and 2.12 $s^{-1}$, respectively) were noticeably higher than that of Pt/C (1.99 $s^{-1}$) at 175 °C. This result indicated that the Pt-Ni alloy catalysts, $Pt_{75}Ni_{25}$/C and $Pt_{50}Ni_{50}$/C in this study, could exhibit the comparable catalytic performance to Pt/C with decreasing Pt content. The enhancement of dehydrogenation activity might be attributed to the electronic structure modification after alloy formation [21–23]. As compared catalytic activity of the prepared catalysts with others reported in literature, our prepared catalysts has a higher catalytic activity in TOF on formic acid decomposition in gaseous phase. For instance, the TOF value of the prepared Pt/C catalyst obtained in this study at 100 °C was 0.23 $s^{-1}$ whereas those of the Pt/C catalyst

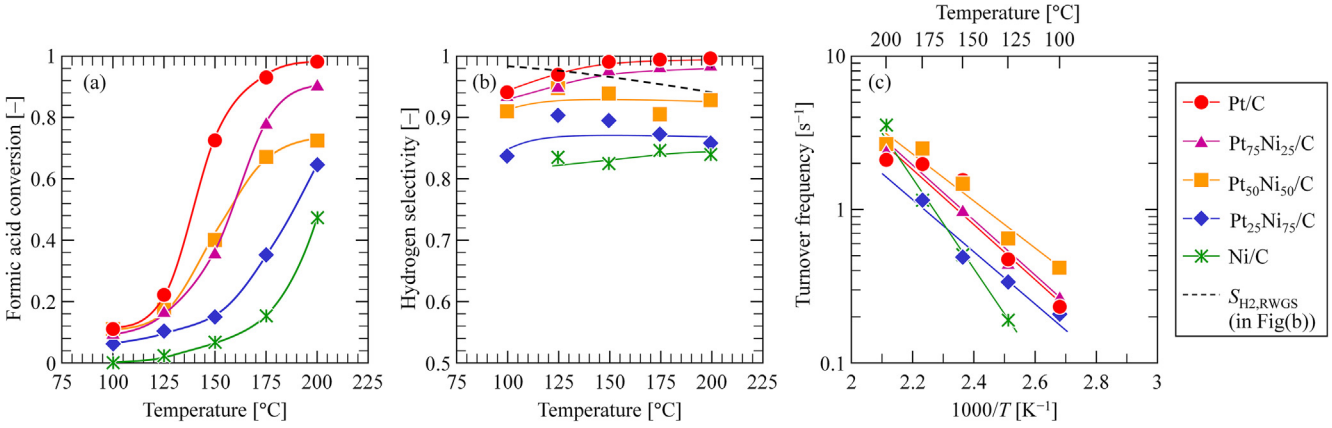


**Fig. 4.** (a) The formic acid conversion, (b) hydrogen selectivity, and (c) Arrhenius plot of turnover frequencies (TOFs) calculated by the active metal surface area measured by CO pulsed chemisorption of the prepared carbon supported Pt-Ni alloy catalysts: Reaction temperature = 100–200 °C; $p_{HCOOH}$ = 12 kPa (with balanced nitrogen); $W/F$ = 0.004 h·$g_{metal}/g_{HCOOH}$.

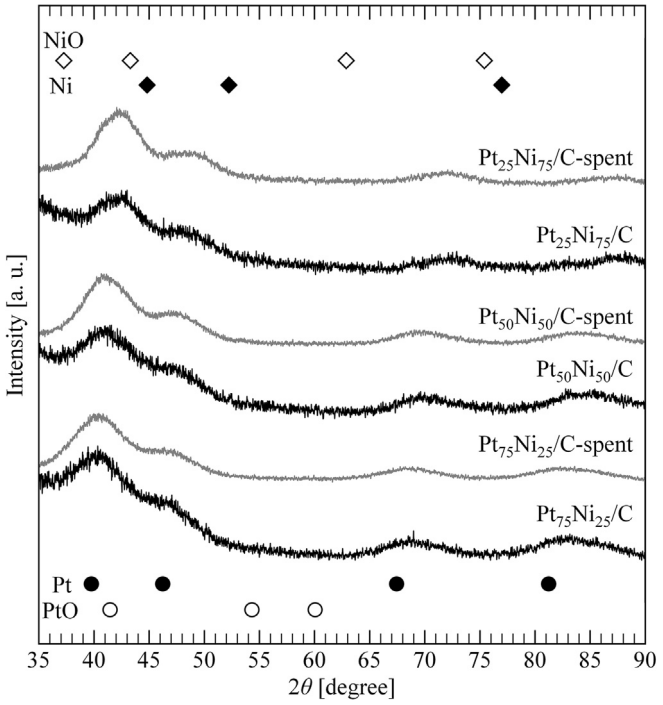


**Fig. 5.** XRD patterns of the fresh and spent carbon supported metal catalysts after formic acid decomposition with characteristic peaks of Pt (●), PtO(○), Ni (◆) and NiO(◊).

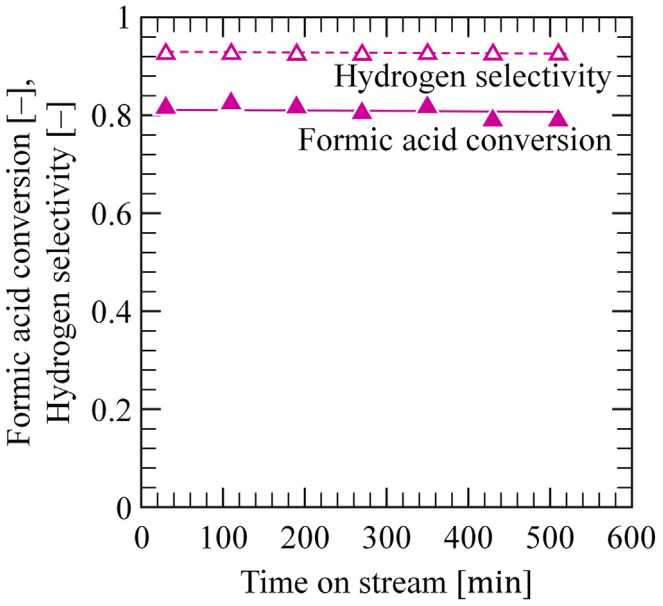


**Fig. 6.** Formic acid conversion and hydrogen selectivity against time on stream over $Pt_{75}Ni_{25}/C$ at 175 °C: $p_{HCOOH}$ = 12 kPa (with balanced nitrogen); $W/F$ = 0.004 h·$g_{metal}/g_{HCOOH}$.

**Table 2**
Metal loading and metal particle of fresh and spent carbon supported metal catalysts after formic acid decomposition.

| | Metal loading [wt%] | $d_{XRD}$ [nm] |
|---|---|---|
| $Pt_{75}Ni_{25}/C$ | 42.8 | 1.8 |
| $Pt_{75}Ni_{25}/C$-spent | 42.9 | 1.7 |
| $Pt_{50}Ni_{50}/C$ | 36.4 | 1.6 |
| $Pt_{50}Ni_{50}/C$-spent | 35.8 | 1.6 |
| $Pt_{25}Ni_{75}/C$ | 31.9 | 2.3 |
| $Pt_{25}Ni_{75}/C$-spent | 31.8 | 2.3 |

previously reported were 0.09–0.18 $s^{-1}$ [5,14]. The higher catalytic activity in TOF was attributed to smaller metal particles of the prepared catalysts. Moreover, the apparent activation energy of formic acid decomposition over the prepared catalysts were estimated from the slope in Fig. 4(c). The yielded apparent activation energy of Pt/C, $Pt_{75}Ni_{25}/C$, $Pt_{50}Ni_{50}/C$, $Pt_{25}Ni_{75}/C$, and Ni/C were 34.8, 35.0, 33.0, 33.7, and 45.4 kJ/mol, respectively. These values were almost half than others obtained in previous studies (70 kJ/mol for Pt/C [5] and 100 kJ/mol for Ni/C [38]). It is well-known that the observed activation energy tends to small when the diffusion process of reactant/product dominantly controls the reaction [39,40]. Because the decomposition activity of the prepared catalysts as high due to the small metal particle size, the diffusion process of formic acid within the pores would affect the overall reaction rate, resulting in apparently low activation energy.

### 3.3. The catalytic activity enhancement by ScWT

To further the improvement of the catalytic activity of the prepared catalysts, ScWT was performed, where the carbon support surrounding the metal particles was gasified by $H_2O$ to form $CO_2$ and CO. According to the preliminary study for the treatment period of the ScWT, the active metal surface area and the accessibility were increased with retaining the metal particle size up to 1 h, while the excess treatment time led to the decreasing of the active metal surface area and the increasing the metal particle size, mainly due to the leaching and the sintering of metals. Thus the optimum treatment time, 1 h, was utilized in this treatment. The properties comparison of the catalysts without and with ScWT at 400 °C for 1 h was summarized in Table 1. Due to the short treatment time, the yield of the catalysts after ScWT was greater than 95% and the catalysts remained their spherical shape and the size. While, the slight increase of the Pt composition was observed by ICP-OES measurement as shown in Table 1, suggesting that a small quantity of Ni dissolved during ScWT. The metal surface area was significantly increased for all the catalysts, indicating that the gasification of the carbon on the active metal proceeded during the ScWT. The metal particle size was not changed as shown in XRD and TEM analyses (Table 2 and Fig. 3(b)). Since the metal surface area increased with retaining fine metal particle size, the metal accessibility substantially increased up to 42.7%. $S_{BET}$, nevertheless, increased only 10–20% and there was no noticeable improvement on micropore volume. The diffraction peaks of the catalysts with ScWT slightly shifted to lower angle, suggesting that the Pt composition was increased by the treatment. This observation was consistent with the ICP-OES result. From this results, the gasification of the carbon support located around metal particles [41] and the leaching of a slight quantity of Ni proceeded during the ScWT resulting in larger metals surface area and slightly higher Pt composition.

To investigate the improvement of catalytic activity by the ScWT at 400 °C for 1 h, hydrogen production via formic acid decomposition over the treated catalysts was performed under the same condition as the untreated catalysts. As illustrated in Fig. 7(a), the significant improvement in formic acid conversion was observed. The conversion of formic acid reached to 100% even at 175 °C over Pt/C-ScWT and $Pt_{75}Ni_{25}/C$-ScWT while it was completed at 200 °C over $Pt_{50}Ni_{50}/C$-ScWT. As described above even though Pt composition increased after ScWT, the enhancement in catalytic activity due to higher Pt composition was considered as a minor effect, as only less than 3.5% of Pt increased whereas metal surface area was almost doubled after ScWT. For instance, the conversion of formic acid reached to 100% at 175 °C over $Pt_{50}Ni_{50}/C$-ScWT, whereas it was only 79% over $Pt_{75}Ni_{25}/C$ even though the amount of Pt in the reactor of $Pt_{75}Ni_{25}/C$ was much higher than that of $Pt_{50}Ni_{50}/C$-ScWT. This evidence pointed out that the enhancement in catalytic activity by ScWT was majorly affected by the

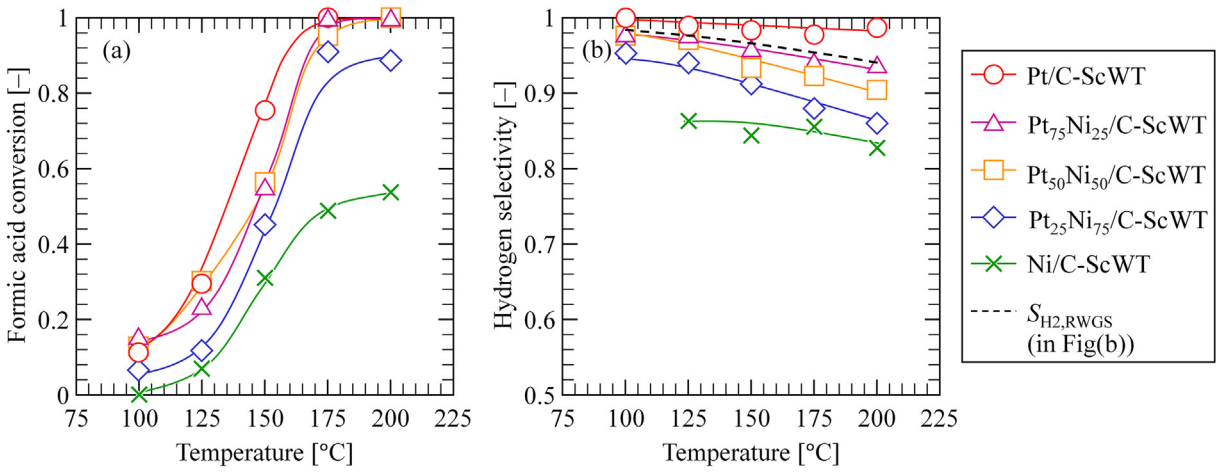


**Fig. 7.** (a) The formic acid conversion and (b) hydrogen selectivity of 1 h the carbon supported Pt-Ni alloy catalysts after ScWT at 400 °C for 1 h: Reaction temperature = 100–200 °C; $p_{HCOOH}$ = 12 kPa (with balanced nitrogen); $W/F$ = 0.004 h·$g_{metal}$/$g_{HCOOH}$.

increasing in the quantity of the active surface metal. On the other hand, the hydrogen selectivity was not significantly changed with and without the treatment (Fig. 7(b)), which might be because that the alloy metal structure was not significantly changed as only little amount of Ni dissolved during the treatment as observed in XRD and ICP-OES.

Moreover, the TOF values on the catalysts with and without the treatment was not significantly improved. For instance, the TOF value of $Pt_{50}Ni_{50}$/C and $Pt_{50}Ni_{50}$/C-ScWT at 150 °C were 1.47 and 1.52 $s^{-1}$, respectively. These results indicate that the enhancement of the catalytic activity of the catalysts with ScWT was mainly due to the increase of the concentration of the active metal sites in the catalysts. The ScWT could therefore be effective to enhance the catalytic activity based on the catalyst volume, leading to the reduction of the reactor volume.

## 4. Conclusion

This study has focused on the preparation of the carbon supported Pt-Ni alloy catalysts by using cation-exchange resin as a carbon material followed by carbonization. Using this preparation method, five compositions of carbon the supported Pt-Ni alloy catalysts, Pt/C, $Pt_{75}Ni_{25}$/C, $Pt_{50}Ni_{50}$/C, $Pt_{25}Ni_{75}$/C, and Ni/C, were successfully prepared at high metal loading (25.4–49.4 wt%) with fine metal particle size (2.7–3.8 nm measured by TEM). The catalytic activity for hydrogen production from formic acid reveals that the conversion in formic acid decomposition increased with increasing Pt composition. Though the Pt/C exhibited the highest formic acid conversion, the TOFs of Pt-Ni alloy catalysts, $Pt_{50}Ni_{50}$/C, and $Pt_{75}Ni_{25}$/C, were higher than that of Pt/C at above 175 °C. This result suggests that the catalytic activity for formic acid decomposition was enhanced by the alloy formation and the Pt-Ni alloy catalysts, namely $Pt_{50}Ni_{50}$/C and $Pt_{75}Ni_{25}$/C, could show comparable catalytic performance with the smaller amount of Pt loading. To further enhancement of the catalytic activity, supercritical water treatment (ScWT) at 400 °C for 1 h was utilized with prepared catalysts. A great improvement was observed in the metal surface area and accessibility, together with no severe metal aggregation and leaching after the treatment. The ScWT was effective to increase the catalytic activity per the catalyst volume, leading to the reactor volume minimization.

## Acknowledgement

This work was partly supported by Yashima Environment Technology Foundation. The authors acknowledge Ookayama Materials Analysis Division from Tokyo Institute of Technology for use of ICP-OES, XRD, SEM, and TEM equipment.

## References

[1] R.M. Navarro, M. Pena, J. Fierro, Hydrogen production reactions from carbon feedstocks: fossil fuels and biomass, Chem. Rev. 107 (2007) 3952–3991.
[2] C.-J. Winter, Hydrogen energy—abundant, efficient, clean: a debate over the energy-system-of-change, Int. J. Hydrogen Energ. 34 (2009) S1–S52.
[3] R. Ramachandran, R.K. Menon, An overview of industrial uses of hydrogen, Int. J. Hydrogen Energ. 23 (1998) 593–598.
[4] M. Balat, Potential importance of hydrogen as a future solution to environmental and transportation problems, Int. J. Hydrogen Energ. 33 (2008) 4013–4029.
[5] F. Solymosi, Á. Koós, N. Liliom, I. Ugrai, Production of CO-free $H_2$ from formic acid. A comparative study of the catalytic behavior of Pt metals on a carbon support, J. Catal. 279 (2011) 213–219.
[6] D.A. Bulushev, S. Beloshapkin, P.E. Plyusnin, Y.V. Shubin, V.I. Bukhtiyarov, S.V. Korenev, J.R. Ross, Vapour phase formic acid decomposition over PdAu/γ-$Al_2O_3$ catalysts: Effect of composition of metallic particles, J. Catal. 299 (2013) 171–180.
[7] C. Hu, J.K. Pulleri, S.-W. Ting, K.-Y. Chan, Activity of Pd/C for hydrogen generation in aqueous formic acid solution, Int. J. Hydrogen Energ. 39 (2014) 381–390.
[8] M. Ojeda, E. Iglesia, Formic Acid Dehydrogenation on Au-Based Catalysts at Near-Ambient Temperatures, Angew. Chem-Ger. Edit. 121 (2009) 4894–4897.
[9] D.A. Bulushev, S. Beloshapkin, J.R. Ross, Hydrogen from formic acid decomposition over Pd and Au catalysts, Catal. Today 154 (2010) 7–12.
[10] D.A. Bulushev, M. Zacharska, A.S. Lisitsyn, O.Y. Podyacheva, F.S. Hage, Q.M. Ramasse, U. Bangert, L.G. Bulusheva, Single atoms of Pt-group metals stabilized by N-doped carbon nanofibers for efficient hydrogen production from formic acid, ACS Catal. 6 (2016) 3442–3451.
[11] C. Tao, W. Guopeng, F. Zhaochi, H. Gengshen, S. Weiguang, Y. Pinliang, L. Can, In situ FT-IR study of photocatalytic decomposition of formic acid to hydrogen on Pt/$TiO_2$ catalyst, Chinese J. Catal. 29 (2008) 105–107.
[12] M.A. Rigsby, W.-P. Zhou, A. Lewera, H.T. Duong, P.S. Bagus, W. Jaegermann, R. Hunger, A. Wieckowski, Experiment and theory of fuel cell catalysis: methanol and formic acid decomposition on nanoparticle Pt/Ru, J. Phys. Chem. C 112 (2008) 15595–15601.
[13] K.L. Miller, C.W. Lee, J.L. Falconer, J.W. Medlin, Effect of water on formic acid photocatalytic decomposition on $TiO_2$ and Pt/$TiO_2$, J. Catal. 275 (2010) 294–299.
[14] L. Jia, D.A. Bulushev, O.Y. Podyacheva, A.I. Boronin, L.S. Kibis, E.Y. Gerasimov, S. Beloshapkin, I.A. Seryak, Z.R. Ismagilov, J.R. Ross, Pt nanoclusters stabilized by N-doped carbon nanofibers for hydrogen production from formic acid, J. Catal. 307 (2013) 94–102.
[15] G. Jacobs, P.M. Patterson, U.M. Graham, A.C. Crawford, A. Dozier, B.H. Davis, Catalytic links among the water–gas shift, water-assisted formic acid decomposition, and methanol steam reforming reactions over Pt-promoted thoria, J. Catal. 235 (2005) 79–91.
[16] G. Jacobs, P.M. Patterson, U.M. Graham, A.C. Crawford, B.H. Davis, Low temperature water gas shift: the link between the catalysis of WGS and formic acid decomposition over Pt/ceria, Int. J. Hydrogen Energ. 30 (2005) 1265–1276.
[17] J. McCarty, J. Falconer, R.J. Madix, Decomposition of formic acid on Ni (110): I. Flash decomposition from the clean surface and flash desorption of reaction products, J. Catal., 30 (1973) 235–249.
[18] R. Joyner, M. Roberts, Photoelectron spectroscopic investigation of the adsorption and catalytic decomposition of formic acid by copper, nickel and gold, Proc. R. Soc. Lond. A 350 (1976) 107–126.
[19] J.B. Benziqer, G.R. Schoofs, Influence of adsorbate interactions on heterogeneous reaction kinetics. Formic acid decomposition on nickel, J. Phys. Chem. 88 (1984) 4439–4444.
[20] J. Benziger, R.J. Madix, The decomposition of formic acid on Ni (100), Surf. Sci. 79 (1979) 394–412.
[21] B. Habibi, N. Delnavaz, Carbon–ceramic supported bimetallic Pt–Ni nanoparticles

as an electrocatalyst for oxidation of formic acid, Int. J. Hydrogen Energ. 36 (2011) 9581–9590.
[22] A.K. Avcı, D.L. Trimm, A.E. Aksoylu, Z.I. Önsan, Hydrogen production by steam reforming of n-butane over supported Ni and Pt-Ni catalysts, Appl. Catal. A: Gen. 258 (2004) 235–240.
[23] M. García-Diéguez, E. Finocchio, M.Á. Larrubia, L.J. Alemany, Characterization of alumina-supported Pt, Ni and PtNi alloy catalysts for the dry reforming of methane, J. Catal. 274 (2010) 11–20.
[24] Y. Shiraishi, D. Ikenaga, N. Toshima, Preparation and catalysis of inverted core/shell structured Pd/Au bimetallic nanoparticles, Aust. J. Chem. 56 (2003) 1025–1029.
[25] M.G. Weir, M.R. Knecht, A.I. Frenkel, R.M. Crooks, Structural analysis of PdAu dendrimer-encapsulated bimetallic nanoparticles, Langmuir 26 (2009) 1137–1146.
[26] M. Navlani-García, K. Mori, M. Wen, Y. Kuwahara, H. Yamashita, Size effect of carbon-supported Pd nanoparticles in the hydrogen production from formic acid, Bull. Chem. Soc. Jpn. 88 (2015) 1500–1502.
[27] B. Liu, H. Li, L. Die, X. Zhang, Z. Fan, J. Chen, Carbon nanotubes supported PtPd hollow nanospheres for formic acid electrooxidation, J. Power Sources 186 (2009) 62–66.
[28] M.S. Saha, R. Li, X. Sun, High loading and monodispersed Pt nanoparticles on multiwalled carbon nanotubes for high performance proton exchange membrane fuel cells, J. Power Sources 177 (2008) 314–322.
[29] S. Ido, H. Nakagawa, K. Miura, Preparation of novel platinum-supported carbon catalysts from ion exchange resin and its application to the combustion of toluene, Carbon (2008) 18D-am-06 (Nagano, 2008).
[30] A. Sharma, H. Nakagawa, K. Miura, A novel nickel/carbon catalyst for $CH_4$ and $H_2$ production from organic compounds dissolved in wastewater by catalytic hydrothermal gasification, Fuel 85 (2006) 179–184.
[31] A. Sharma, H. Nakagawa, K. Miura, Uniform dispersion of Ni nano particles in a carbon based catalyst for increasing catalytic activity for $CH_4$ and $H_2$ production by hydrothermal gasification, Fuel 85 (2006) 2396–2401.
[32] A. Sharma, I. Saito, H. Nakagawa, K. Miura, Effect of carbonization temperature on the nickel crystallite size of a Ni/C catalyst for catalytic hydrothermal gasification of organic compounds, Fuel 86 (2007) 915–920.
[33] C. Cui, L. Gan, M. Neumann, M. Heggen, B.R. Cuenya, P. Strasser, Carbon monoxide-assisted size confinement of bimetallic alloy nanoparticles, J. Am. Chem. Soc. 136 (2014) 4813–4816.
[34] K.-W. Park, J.-H. Choi, B.-K. Kwon, S.-A. Lee, Y.-E. Sung, H.-Y. Ha, S.-A. Hong, H. Kim, A. Wieckowski, Chemical and electronic effects of Ni in Pt/Ni and Pt/Ru/Ni alloy nanoparticles in methanol electrooxidation, J. Phys. Chem. B 106 (2002) 1869–1877.
[35] K. Kim, M.A. Barteau, Structural dependence of the selectivity of formic acid decomposition on faceted titania (001) surfaces, Langmuir 6 (1990) 1485–1488.
[36] K. Tedsree, T. Li, S. Jones, C.W.A. Chan, K.M.K. Yu, P.A. Bagot, E.A. Marquis, G.D. Smith, S.C.E. Tsang, Hydrogen production from formic acid decomposition at room temperature using a Ag–Pd core–shell nanocatalyst, Nat. Nanotechnol. 6 (2011) 302–307.
[37] Q. Luo, G. Feng, M. Beller, H. Jiao, Formic Acid Dehydrogenation on Ni(111) and Comparison with Pd(111) and Pt(111), J. Phys. Chem. C 116 (2012) 4149–4156.
[38] E. Iglesia, M. Boudart, Decomposition of formic acid on copper, nickel, and copper-nickel alloys: I. Preparation and characterization of catalysts, J. Catal. 81 (1983) 204–213.
[39] O. Levenspiel, in Chemical Reaction Engineering, third ed., John Wiley & Sons, New York, 1999 ch. 18.
[40] H.S. Fogler, in Elements of Chemical Reaction Engineering, fourth ed., Prentice Hall International Series in the Physical and Chemical Engineering Sciences, Upper Saddle River, 2006 ch. 12.
[41] A. Kruse, Supercritical water gasification, Biofuels Biofuel Bioprod. Bior. 2 (2008) 415–437.